The Control of Crack Arrays in Thin Films

Jiexi Huang[1], Byoung Choul Kim[2,3], Shuichi Takayama[2,3]
and M. D. Thouless[1,4]
[1]*Department of Mechanical Engineering*
[2]*Department of Biomedical Engineering*
[3]*Macromolecular Science & Engineering Center*
[4]*Department of Materials Science & Engineering*
University of Michigan
Ann Arbor, MI 48109

July 24, 2013

Abstract

Thin-film fracture can be used as a nano-fabrication technique but, generally, it is a stochastic process that results in non-uniform patterns. Crack spacings depend on the interaction between intrinsic flaw populations and the fracture mechanics of crack channeling. Geometrical features can be used to trigger cracks at specific locations to generate controlled crack patterns. However, while this basic idea is intuitive, it is not so obvious how to realize the concept in practice, nor what the limitations are. The control of crack arrays depends on the nature of the intrinsic flaw population. If there is a relatively large density of long flaws, as commonly assumed in fracture-mechanics analyses, reliable crack patterns can be obtained fairly robustly using relatively blunt geometrical features to initiate cracks, provided the applied strain is carefully matched to the properties of the system and the desired crack spacing. This process is analyzed both for cracks confined to the thickness of a film and for cracks growing into a substrate. The latter analysis is complicated by the fact that increases in strain can either drive cracks deeper into the substrate or generate new cracks at shallower depths. If the intrinsic flaws are all very short, the geometrical features need to be very sharp to achieve the desired patterns. While careful control of the applied strain is not required, the strain needs to be relatively large compared to that which would be required to propagate a large flaw across the film. This results in an approach that is not robust against the introduction of accidental damage or a few large flaws.

1 Introduction

Quasi-periodic arrays of cracks often form in layered engineering structures when a brittle film is supported on a substrate [1, 2, 3, 4]. The general features of these arrays depend on the geometry, the properties of the film, interface and substrate, and the tensile strain. However, the details are governed by stochastic factors such as the distribution of the intrinsic flaws, and the sequence in which cracks initiate from these flaws. Crack arrays can be used for nano-fabrication purposes, and some recent experimental examples have been presented in the literature [5, 6, 7, 8, 9]. However, for the potential of these fabrication techniques to be fully realized, the stochastic nature of the cracking has to be eliminated or controlled. Such controlled cracking has been demonstrated in a silicon nitride film deposited on a silicon wafer [10], in a gold film on a poly(dimethylsiloxane) (PDMS) [11], and in the surface layer of oxidized PDMS [11]. While these examples show that it is possible to control crack patterns under some conditions, it is not clear the extent to which these patterns can be robustly controlled. In this paper, we use the mechanics of crack propagation to elucidate the answers to this question, and to provide strategies for controlling crack patterns in different types of materials.

Existing analyses for the formation of crack arrays fall into two groups: shear-lag and linear-elastic fracture mechanics (LEFM) analyses. The shear-lag analyses that consider the statistics of flaw populations [12, 13, 14] were generally developed for studies of crack arrays in laminated composites and the fragmentation of fibers embedded in a matrix, but also apply to the fracture of films on ductile substrates. A characteristic feature of shear-lag analyses is that once a pair of neighboring cracks are close enough to interact, it is impossible to introduce a third crack between them,

no matter what level of strain is applied. If a fully-populated crack array is generated at one unique level of stress (Fig. 1a), these analyses result in the well-known solution to the "car-parking problem" [15, 16] that predicts a crack array with a spacing that varies by a factor of two, and a mean spacing of 1.337 times the smallest spacing. However, this simple result is not valid if the flaws are of different sizes, so that they can be activated by different stress levels (Fig. 1b) [13]. Furthermore, under conditions in which LEFM is appropriate, when there is so little delamination or interfacial slip that it occurs over distances much less than the crack spacing, the maximum stress between two cracks can always be increased by additional loading (Fig. 2c). This means that it is always possible to introduce a third crack between two neighboring cracks, no matter how close they might be, and introduces an aspect of array formation that is missing in shear-lag analyses.

Published fracture-mechanics analyses of crack arrays have all been predicated on the assumption that there is a very high density of long flaws. Furthermore, only characteristic spacings have been obtained [17, 18, 19, 20, 21], with various assumptions about how these might be related to the average spacing. The analyses consider problems in which the cracks are limited to the thickness of the film [17, 18, 19, 20], and those in which they can extend into the substrate [22, 23, 21, 24]. The mechanics of both situations is similar. When the strain in the film is equal to ϵ_o, the characteristic spacing of the array, s_{ch}, is of the form:

$$\frac{s_{ch}}{h} = f_2\left(\alpha, \beta, \frac{\Gamma_f}{\Gamma_s}, \frac{{\epsilon_o}^2 \bar{E}_f h}{\Gamma_f}\right). \tag{1}$$

In this expression, h is the film thickness, Γ is the toughness, the subscripts f and s denote the film and substrate respectively, the Dundurs' parameters for the modulus

mismatch across the interface, α and β are given by [25]

$$\alpha = \frac{\bar{E}_f - \bar{E}_s}{\bar{E}_f + \bar{E}_s} \tag{2}$$

and

$$\beta = \frac{\bar{E}_f(1-\bar{\nu}_s) - \bar{E}_s(1-\bar{\nu}_f)}{2\left(\bar{E}_f + \bar{E}_s\right)}, \tag{3}$$

where $\bar{E} = E/(1-\nu^2)$ and $\bar{\nu} = \nu/(1-\nu)$ in plane strain, E is Young's modulus, and ν is Poisson's ratio. However, the relationship between the characteristic spacing that can be calculated by LEFM and the actual spacings in an array have not been established. It depends on the interaction of two effects: the distribution of the intrinsic flaws responsible for initiating cracks, and the fundamental mechanics of the problem. In particular, LEFM dictates how the energy-release rate for a given flaw depends on both its length and its distance from longer neighboring cracks. The energy-release rate for a crack that is relatively short compared to the film thickness increases linearly with crack length; whereas, the energy-release rate for a relatively long crack scales linearly with film thickness (and is independent of crack length). Similarly, as illustrated in Fig. 2, cracks that are very close to their neighbors have reduced energy-release rates, while cracks that are further away have energy-release rates that are essentially independent of spacing.

The underlying motivation of this paper is to understand possible strategies for controlling crack arrays. The structure of the paper consists of two parts. The first part contains analyses for the creation of uniform arrays, based only on fracture-mechanics concepts and ignoring statistical aspects of the problem. The analyses assume a sufficient density of long flaws, and further assume that the role of any artificial features is to project flaws at their tips sufficiently far to ensure that they will channel preferentially. These analyses are performed for crack arrays confined to

a surface layer, and also for crack arrays that can penetrate into the substrate, as appropriate for stiff films on very compliant substrates. In the second part of this paper, the interaction between thin-film fracture mechanics and the statistics of an intrinsic flaw population is addressed. The model is first used to analyze how natural crack patterns evolve with strain in the absence of geometrical features. It is subsequently used to analyze how artificial geometrical features, the statistics of an intrinsic flaw population, and LEFM can interact to create uniform crack arrays.

2 Fracture mechanics of controlling crack patterns

Fracture-mechanics models without including statistical effects are first used to illustrate a simple strategy for controlling crack patterns. In the following analyses, a uniaxial problem is considered in which cracks are initiated from flaws along a free edge. The lengths of the flaws are sufficient to ensure that the energy-release rates are independent of crack length, and the density of the flaws is sufficient to ensure that cracks will propagate preferentially from wherever the local stress is a maximum. Periodic geometrical features separated by a distance S_o serve to provide locations where the intrinsic flaws extend well beyond their neighbors, since the size of these geometrical features is assumed to be much bigger than the length of any flaw. Cracks will channel preferentially from these features if it is energetically possible to do so. However, if the applied strain is sufficiently small, so that the exclusion length between cracks is greater than S_o, cracks will channel from the tips of only some of the geometrical features. In addition, the flaws along the straight edges of the structure will be in the shadow of the geometrical features, and will not initiate channel cracks. As the strain is increased, more of the geometrical features will be associated with

channel cracks. Eventually, the strain will be so large that the exclusion distance will be less than S_o and, at this point, the shorter defects along the edge can initiate channel cracks. Therefore, tailoring the structure so that the spacing of the geometrical features corresponds to the desired spacing of the crack array requires a delicate balance between the applied strain and the properties of the film and substrate. Too low a strain will result in a random array of cracks initiated from only a limited set of features. Too high a strain will result in random cracks being initiated from flaws away from the features.

These concepts are first illustrated by relatively simple analyses in which the cracks do not penetrate into the substrate. A second case is then considered in which the the cracks can penetrate into the substrate. This second case is complicated by the fact that an increase in strain can either drive existing cracks deeper into the substrate, or cause additional cracks of unknown depth to channel across the system. However, it will be seen that the two processes occur in sequence, so that only when a crack array has reached a critical depth (relative to its spacing) do additional cracks form.

2.1 Crack arrays limited to the film

The calculations were done by computing the energy change associated with channeling a crack between two existing cracks separated by a distance of $2s$ in a film of thickness h. Although standard fracture-mechanics results from Tada *et al.* [26] can be used to analyze a homogeneous system, numerical calculations are required when the effects of a modulus mismatch are included. These calculations were done using the commercial finite-element code ABAQUS. Mesh-sensitivity analyses were

conducted as part of the process to determine the magnitude of the numerical uncertainties, the magnitudes of which are reflected in error bars on the resulting plots when they are significant.

Two geometries were used in the calculations (Fig. 3). One geometry (Fig. 3a) was used to calculate the stress distribution $\sigma(y)$ along the mid-plane between two cracks of depth h and a distance $2s$ apart for a given value of applied strain, ϵ_o. The second geometry, had a third crack, also of depth h, exactly in the middle, with surface tractions corresponding to $-\sigma(y)$ applied along its surface. The resulting crack-opening displacements, $u(y)$, were computed, and the steady-state energy-release rate for channeling this new crack, $\mathcal{G}_{ss}$, was calculated from [27]

$$\mathcal{G}_{ss} = \int_0^h \sigma(y)u(y)dy/h. \tag{4}$$

This integral was computed numerically from the output of the finite-element calculations. From this result, the condition for whether the new crack can channel was calculated by comparing the energy-release rate to the toughness of the film, Γ_f.

The final step of the calculations involved equating the separation, S_o, of the geometrical features to $2s$. When S_o is sufficiently large to permit a new crack to channel between two existing cracks, a random crack array will be generated, because cracks can be formed away from the geometrical features. Conversely, if $2S_o$ is smaller than the distance that will allow an intermediate crack to propagate, then not every feature will have a crack associated with it and, again, there will be a random aspect to the crack pattern. There will, however, be a "Goldilocks" regime which is "just right" for propagating cracks from every feature, but no more. This regime is shown in the two plots of Fig. 4: one calculated with no modulus mismatch between the

film and substrate (Fig. 4a), and one with a mismatch (Fig. 4b). It corresponds to a range of strains between the minimum value required to permit cracks to channel at a separation of S_o and the maximum value that is just too low to permit cracks to channel at a separation of $S_o/2$. This range is what allows one to realize perfectly periodic arrays with careful matching between the feature separation, the properties of the material, and the applied strain. From Fig. 4 it can be seen that the range of strains for periodic arrays increases as the feature separation decreases; it also increases with increasing modulus mismatch.

The conclusions are consistent with the experimental observations described by Kim *et al.* [11]. In their study, "V"-shaped notches were formed in poly(dimethylsiloxane) (PDMS) substrates with a separation of 48 μm using soft lithographic techniques. Specifically, a 5:1 mixture of the curing agent and PDMS (Sylgard 184, Dow Corning) was cast against silicon moulds and cured at 60°C. The surface was plasma treated to create a thin surface layer of a relatively brittle silica-like material. While the material properties of this surface layer are not well-characterized, there is evidence that the modulus is only slightly higher than that of the substrate, and the cracks remain within the surface layer [8].

Figure 5 shows how a systematic increase in the applied strain resulted in a crack pattern for the system that evolved from (i) random cracking at some of the notches, through (ii) periodic cracking at every notch, to (iii) random cracking at locations away from the notches. In this system, the range of strains for periodic cracking was very narrow, with a value of the critical strain of approximately 6%. Based on earlier work, the thickness of the surface layer can be estimated as being about 200 nm [8]. This makes the value of S_o/h equal to about 240. As can be seen from Fig. 4a,

when $S_o/h > 100$ the strain range for periodic cracks is, indeed, vanishingly small, which is consistent with what was observed for the plasma-treated PDMS. The predicted strain required for periodic cracks in a homogeneous system with this spacing is about $\epsilon_o\sqrt{\bar{E}_f h/\Gamma_f} = 0.71$. Again, using the results of Mills *et al.* [8], the modulus of the surface layer can be taken to be about 25 MPa, and the toughness can be taken to be about 200 mJ/m^2. This would suggest a critical strain of about 14%. While this is greater than the measured value, it should be noted that all the material parameters for the plasma-treated layer are known to only very approximate levels, and the observed strain levels are well within any uncertainties of the predicted values.

2.2 Crack arrays penetrating into the substrate

A large modulus mismatch, such as that between a gold film and PDMS, results in crack arrays penetrating relatively deep into the substrate [24]. This complicates the analysis because an increase in strain can result in two possible events: (i) the growth of existing cracks deeper into the substrate, or (ii) the channelling of intermediate cracks of unknown depth. In this section, a fracture-mechanics analysis is presented to determine the conditions required to control such crack arrays.

The analysis was done in a similar fashion to that of the previous section using ABAQUS to perform the numerical calculations. In the first step of the calculations (Fig. 6a), the applied strain required to propagate two cracks of depth a_o, penetrating through a film of thickness h and separated by a distance $2s$, deeper into the substrate was determined. This was done by computing the energy-release rate at the tips of the cracks, and equating the value of this parameter to the toughness of the substrate, Γ_s. The stress distribution, $\sigma(y)$, along the mid-plane between these two cracks was

computed for this strain level. In the next step (Fig. 6b), a crack was introduced along this plane to an arbitrary depth, a, with surface tractions corresponding to $-\sigma(y)$ along its surface. The corresponding crack-opening displacements, $u(y)$, were calculated, and the energy-release rate for channelling calculated from

$$\mathcal{G}_{ss} = \int_{h-a}^{h} \sigma(y)u(y)dy/a. \tag{5}$$

This energy-release rate was then compared to the effective toughness for a crack channeling at a depth a, which is given by

$$\Gamma = (h/a)\Gamma_f + (1 - h/a)\Gamma_s, \tag{6}$$

to find whether there was any value of a for which an intermediate crack could channel between the other two cracks. If it was not possible to form a secondary crack, the applied strain was increased, and a new equilibrium crack depth was determined for the original cracks.

The calculations were repeated until a secondary crack could channel at any depth. At this stage, the calculations were repeated for all three cracks (Fig. 7), exploring the possibilities of either introducing another set of intermediate cracks or growing the existing cracks. These calculations revealed the sequence of cracking for this problem. The intermediate crack is first formed at a shallower depth than the original pair of cracks, and immediately unloads the original cracks. While a further increase in strain increases the energy-release rate at the tips of all the cracks, only the shallower intermediate crack meets the condition to grow deeper. Eventually, it reaches the depth of the original cracks. Furthermore, during this stage, it is not thermodynamically possible to introduce any further intermediate cracks. Once all cracks are at the same depth, a further increase in strain allows the entire set to propagate deeper,

until eventually another set of shallow intermediate cracks can channel, and the entire sequence is repeated.

Following the approach and assumptions of the previous section, Fig. 8 shows the range of strains for which the crack spacing will match that of the geometrical features in a system for which the film modulus is 10^4 times higher than the substrate modulus, so that $\alpha = 0.9998$ and $\beta = 0$, and the film-to-substrate toughness ratio, Γ_f/Γ_s, is 35. This figure shows the same important conclusions that are evident from Fig. 4. There is a limited range of strains over which periodic cracking can be reliably obtained; channel cracks will be initiated at only some of the features if the strain is too low, and they will be initiated from sites away from the features if the strain is too high.

A new aspect of the problem is the prediction of how the crack depths evolve within the regime where the crack spacing matches the feature spacing. Figure 9 shows how the crack depths are initially bimodal at the lowest strain for which uniform cracking is obtained, with the newest cracks being shallower than the original ones. An increase in strain results in the growth of the new cracks, while the original cracks remain at their original depth (assuming no healing), until all the cracks are of the same depth. From this point on, an increase in strain causes all the cracks to grow deeper in a uniform fashion, until a new set of cracks is introduced. The numerical predictions for the crack depth are very sensitive to the ratio of the film toughness to the substrate toughness, Γ_f/Γ_s. Deeper cracks occur for larger values of this ratio. The results shown in Figs. 8 and 9 are based on a value of $\Gamma_f/\Gamma_s = 35$, resulting in relatively deep cracks.

Experimental observations of Kim *et al.* [11] (Fig. 10) confirmed that the three cracking regimes are observed when there is a huge modulus mismatch between the film and substrate, and the channeling cracks propagate far below the interface [24]. A similar process to that described in the previous section was used to fabricate a PDMS substrate with notches in it. A 10 nm adhesion layer of Cr was deposited by e-beam on the surface of the PDMS, followed by a 40 nm thick Au layer. The results shown in Fig. 10 are for for notches separated by 238 μm. This corresponds to a value of S_o/h of about 5000. Laser interferometry confirmed that the cracks which formed upon the application of a tensile strain were approximately 3 microns deep, or about 60 times deeper than the total film thickness.

While the experimental tri-layer system of Au/Cr/PDMS does not exactly match the geometry or the modulus mismatch ratio assumed in developing the mechanics results of Fig. 8 and 9, an approximate quantitative comparison can be made. In contrast to the results for the plasma-treated PDMS, the uniform cracking regime existed over a relatively wide range of strains from about 10% to just under 20%. If the toughness, Γ_s and modulus, $\bar{E}_s$ of the PDMS substrate are taken to be about 240 J/m^2 and 4.5 MPa [8], this results in a range of normalized strains, $\epsilon_o\sqrt{\bar{E}_s h/\Gamma_s}$, for periodic cracking of 0.003 to 0.006. The calculations of Fig. 8 indicate that for $S_o/h = 5000$, the corresponding range of normalized strains is 0.002 to 0.004. Within the range of uncertainty for all the parameters, this provides relatively good consistency between the analysis and experimental observations.

One important parameter that is not well characterized in the experiments is the toughness of the film. In particular, it should be noted that a relatively tough film is required to predict crack depths that are consistent with the experimental observa-

tions. However, thin metal films with the dimensions used in this study are expected to have very low values of toughness, because of the lack of volume in which to develop a plastic zone. This paradox can be resolved by recognizing that a PDMS substrate will provide very little constraint to plastic deformation of the film and that,without such a constraint, thin metal films can rupture by shear localization [28] upon yield at very high strains. Cracking of these systems is probably initiated by shear localization when the metal film reaches the yield strain. In particular, it should be noted that the results of Figs. 8 and 9 are reproduced exactly if the calculations are repeated with the coupled assumptions that $\Gamma_f/\Gamma_s = 0$ and that cracks cannot form unless the strain in the film equals 1%. This would seem to be the appropriate form in which the calculations should be conducted for very thin, high-strength metal films supported on compliant substrates.

3 Statistical effects on crack arrays

In this section, statistical aspects are considered to investigate how crack arrays are affected by the distribution of flaw sizes and density. The calculations were done by performing Monte Carlo simulations on a homogeneous system with a film of thickness h, in which cracks did not penetrate the substrate. Before investigating the effect of geometrical features on array formation, an analysis of how natural crack arrays are generated in uniform structures was done as a point of comparison. While shear-lag analyses have been coupled with statistics[12, 13, 14], a coupling between thin-film linear-elastic fracture mechanics and flaw statistics has not been presented before. Even for flaw populations that meet the conditions usually assumed (dense, long flaws), fracture-mechanics analyses cannot predict the sequence in which crack

arrays form, nor what the mean spacing of an array might be. This information can only be obtained by incorporating some statistical aspects into the analysis, even in the case when all the flaws are so long that LEFM would predict that each individual flaw on its own would propagate at the same stress level.

In the simulations presented here, the intrinsic flaws were assumed to be distributed uniformly along the edge with a density of ρ per unit length. The lengths of the flaws were assumed to follow a Gaussian distribution centered about zero with a standard deviation of μ, but truncated to the interval of $(0, \infty)$. This truncated distribution resulted in a monotonically decreasing probability of large flaws, with the mean length of the flaws scaling with μ. The simulations were done for a specimen of finite length L; but, it was verified empirically that L was always large enough so as not to affect the results in a significant fashion.

Three parameters determine the energy-release rate to channel a crack in a thin film: (i) the local strain, (ii) any shielding that may be provided by neighboring cracks, and (iii) the length of the flaw. In order to simplify the analysis, various assumptions were made about these parameters. Any flaws on the edge of geometrical features were assumed to experience a local strain, ϵ_l, that was elevated above the remote applied strain, ϵ_o, according to the Inglis solution for the stress concentration at the surface of an ellipse [29]. The effect of shielding was assumed to be determined by the distance to the nearest crack (or geometrical feature) that extended beyond the tip of the crack being analyzed. Figure 11 shows examples of how this closest spacing was determined. The appropriate energy-release rate for an individual flaw was then calculated from the local strain and this distance, making a further approximation

that the flaw was equidistant to two neighbors at this minimum spacing.[1] Figure 2 was used to determine an empirical equation for the relationship between the channeling energy-release rate, $\mathcal{G}$, for a long crack, the local strain, ϵ_l, the film thickness, h, and the distance, d, to the nearest (longer) neighbor:

$$\frac{\mathcal{G}}{\bar{E}_f \epsilon_l^2 h} = 1.98(1 - e^{-0.172d/h}). \tag{7}$$

Here, the modulus of the film, $\bar{E}_f$, has been assumed to be identical to the modulus of the substrate. The channeling energy-release rate for a short crack of length a was assumed to be equal to the energy-release rate at the tip of a two-dimensional edge crack [26], with the effect of crack spacing being of the same functional form as for long cracks, so that

$$\frac{\mathcal{G}}{\bar{E}_f \epsilon_l^2 h} = 1.25\pi \frac{a}{h}(1 - e^{-0.172d/h}). \tag{8}$$

The calculations proceeded by seeding the geometry of interest with cracks having a statistical distribution of lengths, evaluating the distance, d, to the nearest longer neighbor for each crack, and using this distance to calculate the energy-release rate for the crack as being the smallest of either Eqn. 7 or 8. The energy-release rate was then compared to the toughness of the film, so as to determine whether a crack would channel at a given level of strain. With a linear-elastic system, the calculations for any individual crack only needed to be performed once, since it was assumed that the energy-release rate was not affected by the growth of any nearest longer crack. (The shielding effect of a neighboring longer crack was assumed to be unchanged by growth of the neighbor.)

[1] This approximation could be relaxed by doing a series of calculations for the energy-release rate of cracks not spaced symmetrically between two other cracks. However, it is not expected that this would have a significant affect on the results.

3.1 Crack arrays without geometrical features

The first set of results are presented for a geometry with no artificial features and subjected to a uniform strain of ϵ_o. Figure 12 shows how the cumulative distribution function for the crack spacing varies with strain for the limiting case of a relatively high density of large intrinsic flaws. This is the appropriate condition for making comparisons to LEFM results for characteristic spacings. The average spacing for this flaw population is shown as a function of applied strain in Fig. 13 (solid line). Consistent with the results for the characteristic spacing from LEFM solutions, the cracks first form at a normalized strain of $\epsilon_o\sqrt{\bar{E}_f h/\Gamma_f} = 0.71$, and the crack spacing decreases with increases in applied strain. It should be emphasized that this change in spacing occurs even though the flaws are long enough for there to be no effect of size on strength. This provides a contrast to crack-spacing models based on Weibull statistics which inherently assume a locally varying coating strength dependent on the flaw size. The results of Fig. 13 indicate that, away from the threshold strain, the mean spacing, s_{av}, for the statistical distribution assumed in this paper is approximately given by

$$s_{av}/h \propto \left(\epsilon_o\sqrt{\bar{E}_f h/\Gamma_f}\right)^{-2.36}. \tag{9}$$

This is a steeper relationship than the inverse linear forms that result from analyses based either on the minimum spacing that just prevents an intermediate crack from channeling [19] or on a consideration of equilibrium [18, 20]. It is expected that this relationship may be sensitive to the form of the assumed flaw population, through how the distribution controls the distance to nearest longer neighbors, but this detail of the problem has not been explored.

The effects of flaw density and length, and of strain and toughness on the average spacing of the array are also shown in the plots of Fig. 13. The details of this plot would vary with different forms of the flaw distribution and on the material properties; but, the general mechanics concepts will apply. While the onset of channeling always occurs at a normalized strain of 0.71 for a homogeneous system, a limited density of longer flaws increases the spacing for a given level of strain. The asymptotic spacing that is shown for some flaw populations at large strains is simply a consequence of an assumption that there is a finite set of flaws that can initiate channel cracks.

3.2 The effect of geometrical features on crack arrays

The second set of results shows the effect on crack arrays of geometrical features consisting of periodic elliptical cut-outs spaced at S_o along the edge of the specimen. Each elliptical hole is assumed to have a minor radius, b, aligned with the flat edge, and a major radius of a. To simplify the process of seeding flaws in the analysis, it was assumed that the density, ρ, is given in terms of the projected length along the flat edge, rather than the actual length of the surface. The flaws were assumed to be perpendicular to the straight edge. As shown in Fig. 11, the distance used to calculate the energy-release rate was the distance from the tip of each flaw to the nearest intersection with either a flaw or the surface of an ellipse. The Inglis solution for an ellipse [29] was used to calculate the local strain from which the energy-release rates for a flaw along the surface of a cut-out could be calculated. However, an additional consideration in this problem was to determine whether such a crack could continue channeling once it left the stress concentration at the tip of the ellipse. This was done by a second step in which the energy-release rate for any flaw along the surface of an ellipse that had been determined to meet the conditions of growth was recalculated

with the assumption that it had reached a steady-state length but was out of the stress-concentration region. If a crack didn't meet this second growth condition, it was assumed to have propagated only a little way from the geometrical feature, and not to have channeled across the specimen. It was, therefore, not counted as forming the crack array. (However, it was possible for these cracks to channel subsequently at a higher level of applied strain.)

Cumulative distribution functions for a structure with a dense population of relatively large flaws are shown in Fig. 14. There are three points to be observed in these plots. First, consistent with the fracture-mechanics calculations of Section 2, there are three regimes of crack arrays: (i) at low strains, relatively few cracks channel across the system, and not every geometrical features initiates a crack; (ii) at intermediate strains, the distribution has a sharp and single edge corresponding to the spacing of the geometrical features; (iii) at high strains, a significant number of cracks can form between the geometrical features, resulting in a non-uniform distribution again. Second, the range of strains over which this single mode of crack spacings can be obtained is very sensitive to the chosen value of S_o, becoming very restricted at large values of S_o. Third, the results are not very sensitive to the aspect ratio of the geometrical features. These conclusions are all consistent with the observations of Kim *et al.* [11] for an oxidized PDMS system, which supports the notion that this system was one with relatively large intrinsic flaws that could be analyzed by conventional LEFM approaches for thin films, described in the previous section.

Figure 15 presents some cumulative distribution functions for a structure with very small intrinsic flaws. A key feature to be noticed from these plots is that the strains required to ensure the initiation of a crack from every geometrical feature

are greater than the strains required to channel cracks from long flaws between the geometrical features. So, the formation of uniform arrays in these systems relies on the absence of any significant flaws between the geometrical features. Since it relies on controlling the statistics of the flaw population, the approach can be considered to be rather unstable, and damage can trigger much finer arrays than intended. Sharper geometrical features lower the critical strains required to form periodic arrays, and, at a given strain, a uniform array is more likely to be formed with sharper features. Both of these conclusions, the sensitivity of array formation to the aspect ratio of the features, and the triggering of uncontrolled arrays by unintended damage, are consistent with the experimental observations presented by Nam *et al.* [10].

The strategy for forming periodic patterns when there is a sufficient density of relatively large flaws is robust against damage, and is not very sensitive to the nature of the geometrical features, but it can require a careful matching of the strain to the desired spacing, depending on the modulus-mismatch ratio. The strategy of relying on the intrinsic flaws being very small is sensitive to the aspect ratio of the features, but may not be so sensitive to the strain. However, this strategy is vulnerable to unintended damage. A lack of strain sensitivity is useful in that it allows a range of crack spacings to be generated on a single specimen. This versatility can be obtained either by keeping the density of long flaws low, or by ensuring that the film has a much higher modulus than the substrate.

4 Conclusions

The stochastic nature of flaws affects the formation of crack arrays in linear-elastic systems through the fact that the energy-release rate for channeling a crack depends on its distance to nearest longer neighbors. This introduces a statistical aspect of crack lengths to the problem, even if all the flaws are long enough so that the energy-release rates are insensitive to their lengths. This is a different effect from the more usual assumption (used in Weibull statistics, for example) that the statistics of crack lengths enter fracture problems directly through the dependence of energy-release rates on crack length. These two aspects of the effects of statistics on cracking give rise to two distinct approaches for controlling the formation of crack arrays: one relies on maintaining a sparse density of flaws, the other is more general and applies to systems with fairly extensive flaw populations.

Controlled arrays can be generated in a system with very small flaws by introducing sharp geometrical features that trigger crack channeling from small defects at points of high stress concentrations. While there can be considerable latitude for the range of strains that can be used with this technique, the strains have to be relatively high, and the strategy is not stable against any accidental introduction of additional large defects. The control of the crack array using this strategy is very sensitive to the details of the strain enhancement. The physics behind this proposed strategy seems to be consistent with the reported observations concerning controlled crack patterns in a silicon nitride film deposited on a silicon wafer [10]. In that paper, evidence was given that the crack patterns could be controlled, but the details of the stress concentrators used to trigger cracks were important. There was also evidence that the system failed occasionally, with dense random arrays being generated.

Controlled arrays can also be generated in systems with relatively large defect populations by introducing geometrical features. The role of these features is to project the tips of some flaws well beyond the others at well-defined points where channeling is desired. These cracks propagate first, when the appropriate strain conditions are met. Since the role of the features is primarily to shield flaws from which cracks should not channel, less stringent conditions are placed on their sharpness than on the features discussed in the previous paragraph. However, the design of the system requires a tight coupling between the material properties of the system, the geometry, and the applied strain used to generate the crack arrays. A small difference in modulus between the film and substrate allows only relatively close crack spacings to be obtained reliably. A large difference in modulus mismatch, which can be accompanied by cracking of the substrate, allows a larger range of crack spacings, and a larger range of strains over which the spacings can be matched correctly.

This strategy of strain matching is consistent with observations on the formation of controlled crack patterns on oxidized PDMS and in gold films deposited on PDMS [11]. This system has been used as the basis for fabricating tunable nanochannels used for confining DNA and chromatin [9]. It is believed that the strategy outlined in this paper can be used to ensure uniform arrays, so that at a given strain all the channels in an array will have similar dimensions. One question that might arise is whether the cracks in an initially uniform array will close in a uniform fashion, or whether some cracks might collapse before others. In this regard, it should be noted that the appropriate toughness for healing these arrays (corresponding to a physical attraction, such as van der Waals) will be much lower than the toughness associated with crack formation. Therefore, the arrays that form are very sparse

compared to the natural spacing that would correspond to the toughness appropriate for the healing process. This means that the cracks will not interact with one another until the applied strain has been relaxed to very low levels, and the closing of the nano-channels should be effectively uniform until the system is almost completely strain free. This is consistent with optical observations in these systems, and suggests that, once formed, uniform crack arrays in compliant systems should provide repeated consistent opening and closing cycles if required.

Acknowledgments

This work was done as part of an effort to develop tunable nano-channels for biomechanics applications, and the authors gratefully acknowledge support from the National Institute of Health (R01-HG004653-01).

References

[1] G. Gille. Strength of thin films and coatings. In E. Kaldis, editor, *Current Topics in Materials Science*, volume 12, pages 421–472. North Holland (Elsevier), Amsterdam, Netherlands, 1985.

[2] M. S. Hu and A. G. Evans. The cracking and decohesion of thin films on ductile substrates. *Acta Metallurgica*, 37:917–925, 1989.

[3] D.C. Agrawal and R. Raj. Measurement of the ultimate shear strength of a metal-ceramic interface. *Acta Metallurgica*, 37:1265–1270, 1989.

[4] E. Olsson, A. Gupta, M. D. Thouless, A. Segműller and D. R. Clarke. Crack formation in epitaxial [110] thin films of $YBa_2Cu_3o_{7-\delta}$ and $PrBa_2Cu_3O_{7-x}$ on [110]$SrTiO_3$ substrates. *Applied Physics Letters*, 58:1682–1684, 1991.

[5] R. Adelung, O. C. Aktas, J. Franc, A. Biswas, R. Kunz, M. Elbahri, J. Kanzow, U. Schürmann and F. Faupel. Controlled growth of nanowires within thin-film cracks. *Nature Materials*, 3:375–379, 2004.

[6] X. Zhu, K. L. Mills, P.R. Peters, J. H. Bahng, E. H. Liu, J. Shim, K. Naruse, M. E. Csete, M. D. Thouless and S. Takayama. Fabrication of reconfigurable protein matrices by cracking. *Nature Materials*, 4:403–406, 2005.

[7] D. Faruqui and A. Sharma. Stress engineered polymeric nanostructures by self-organized splitting of microstructures. *Industrial Engineering and Chemical Research*, 47:6374–6378, 2008.

[8] K. L. Mills, D. Huh, S. Takayama and M. D. Thouless. Instantaneous fabrication of arrays of normally closed, adjustable, and reversible nanochannels by tunnel cracking. *Lab on a Chip*, 10:1627–1630, 2010.

[9] T. Matsuoka, B. C. Kim, J. Huang, N. J. Douville, M.D. Thouless and S. Takayama. Nanoscale squeezing in elastomeric nanochannels for single chromatin linearization. *Nano Letters*, 12:6480–6484, 2012.

[10] K. H. Nam, I. H. Park and S. H. Ko. Patterning by controlled cracking. *Nature*, 485:221–224, 2012.

[11] B. C. Kim, T. Matsuoka, C. Morales, J. Huang, M.D. Thouless and S. Takayama. Guided fracture of films on soft substrates to create micro/nano-feature arrays with controlled periodicity. *Scientific Reports*, under review, 2013.

[12] R. B. Henstenburg and S. L. Phoenix. Interfacial shear strength studies using the single-filament-composite test. part ii: A probability model and monte carlo simulation. *Polymer Composites*, 10:389–408, 1989.

[13] W. A. Curtin. Fiber fragmentation in a single-filament composite. *Applied Physics Letters*, 58:1155–1157, 1991.

[14] M. Heinrich, P. Gruber, S. Orso, U. A. Handge and R. Spolenak. Dimensional control of brittle nanoplatelets. a statistical analysis of a thin film cracking approach. *Nano Letters*, 6:2026–2030, 2006.

[15] A. C. Kimber and J. G. Keer. On the theoretical average crack spacing in brittle matrix composites containing continuous aligned fibres. *Journal of Materials Science Letters*, 1:353–354, 1982.

[16] X. F. Yang and K. M. Knowles. The one-dimensional car parking problem and its application to the distribution of spacings between matrix cracks in unidirectional fiber-reinforced brittle materials. *Journal of the American Ceramic Society*, 75:141–147, 1992.

[17] M. D. Thouless. Crack spacing in brittle films on elastic substrates. *Journal of the American Ceramic Society*, 73:2144–2146, 1990.

[18] M. D. Thouless, E. Olsson and A. Gupta. Cracking of brittle films on elastic substrates. *Acta Metallurgica et Materialia*, 40:1287–1292, 1992.

[19] J. W. Hutchinson and Z. Suo. Mixed mode cracking in layered materials. *Advances in Applied Mechanics*, 29:63–191, 1992.

[20] V. B. Shenoy, A. F. Schwartzman and L. B. Freund. Crack patterns in brittle thin films. *International Journal of Fracture*, 103:1–17, 2000.

[21] M. D. Thouless, Z. Li, N. J. Douville and S. Takayama. Periodic cracking of films supported on compliant substrates,. *Journal of the Mechanics and Physics of Solids*, 59:1927–1937, 2011.

[22] T.-Y. Zhang and M.-H. Zhao. Equilibrium depth and spacing of cracks in a tensile residual stressed thin film deposited on a brittle substrate. *Engineering Fracture Mechanics*, 69:589–596, 2002.

[23] T. Ye, Z. Suo and A. G. Evans. Thin film cracking and the roles of substrate and interface. *International Journal of Solids and Structures*, 29:2639–2648, 1992.

[24] N. Douville, Z. Li, S. Takayama and M. D. Thouless. Crack channelling in a metal-coated elastomer. *Soft Matter*, 7:6493–6500, 2011.

[25] J. Dundurs. Edge-bonded dissimilar orthogonal elastic wedges. *Journal of Applied Mechanics*, 36:650–652, 1969.

[26] H. Tada, P. C. Paris and G. R. Irwin. *The Stress Analysis of Cracks Handbook, 3rd ed.* The American Society of Mechanical Engineers, New York, NY, 2000.

[27] J. L. Beuth, Jr. Cracking of thin films bonded in residual tension. *International Journal of Solids and Structures*, 29:1657–1675, 1992.

[28] D. W. Pashley. A study of the deformation and fracture of single-crystal gold films of high strength inside an electron microscope. *Proceedings of the Royal Society*, A255:218–231, 1960.

[29] C. E. Inglis. Stresses in a plate due to the presence of cracks and sharp corners. *Proceedings of the Institute of Naval Architects*, 55:219–230, 1913.

Figure Captions

Figure 1: **(a)** If there is a single value for the cracking strength, a shear-lag model predicts the formation of a crack array at one level of the applied stress, and the crack spacing is given by the solution to the "car parking" problem. **(b)** If there are multiple cracking strengths, a shear-lag model predicts an increasing density of cracks until a saturated array is formed. **(c)** In an elastic problem, the stresses can continue increasing between two cracks, and further cracks can always channel between them, provided there is a suitable flaw to initiate the crack.

Figure 2: The energy-release rate for channeling a crack across the surface of a film depends on the distance to its two nearest neighbors (assumed to be equi-distant in this plot).

Figure 3: A schematic showing the process by which the energy changes associated with a crack channeling between two pre-existing cracks are calculated. In **(a)**, the stress distribution $\sigma(y)$ along the mid-plane between two cracks at a distance $2s$ apart is calculated for an applied strain of ϵ_o. In **(b)**, a crack is introduced along this plane, with surface tractions corresponding to $-\sigma(y)$ applied along the new crack surface, and the resultant crack opening displacements $u(y)$ are calculated.

Figure 4: Plots showing the regimes of strains and feature spacing in which periodic crack arrays contained within the film can be obtained for **(a)** a film with no modulus mismatch, and **(b)** a film with a modulus mismatch corresponding to a value of $\alpha = 0.98$, and $\beta = 0$. (The film-to-substrate thickness ratio is 10^{-4}.)

Figure 5: Micrographs showing the three regimes of cracking for an oxidized structure made from PDMS, with a feature separation of 48 μm. As the strain is increased, **(a)** a random array with too few cracks is first formed, then **(b)** a periodic array corresponding to a single crack initiating from each geometrical feature is formed, and finally **(c)** additional cracks propagate from between the geometrical features. The region of interest for crack formation is in the middle of the micrographs, between the geometrical features. This region is isolated from the rest of the structure by the channel that forms the geometrical features. The cracks that can be seen outside this region of interest were triggered from random flaws elsewhere in the system. Since they are isolated from the array of interest, they have no effect upon it.

Figure 6: A schematic showing the process by which the energy changes associated with channeling a crack that penetrates into the substrate between two existing cracks of depth a_o, separated by a distance $2s$. In **(a)**, the strain that would just cause the existing cracks to penetrate deeper into the substrate is determined. The stress distribution, $\sigma(y)$, along the mid-plane between these two cracks is computed for this strain level. In **(b)**, a crack is introduced to an arbitrary depth a, with surface tractions corresponding to $-\sigma(y)$ along its surface. The corresponding crack-opening displacements, $u(y)$, are calculated.

Figure 7: The secondary crack of depth a_2 is initially shallower than the primary cracks that reach a depth of a_1 before it is energetically favorable for the secondary crack to form. A second set of calculations is then required to compute which cracks will grow, and the conditions for when a tertiary

set of cracks can channel between the other two sets.

Figure 8: A graph of strains over which periodic arrays of cracks can be obtained. An identical figure is obtained if the calculations are repeated with $\Gamma_f/\Gamma_s = 0$, but the cracks can not form unless the strain in the film is 1%. (The film-to-substrate thickness ratio is 10^{-4}.)

Figure 9: Plots of how the crack depths vary with strain within the regime for which there is a uniform crack spacing. The solid lines correspond to the primary cracks, and the dashed lines correspond to the secondary cracks formed at the beginning of each strain range. (The film-to-substrate thickness ratio is 10^{-4}.)

Figure 10: Micrographs showing the three regimes of cracking for a sample of PDMS coated with a 10 nm Cr layer (used as an adhesion layer) and 40 nm of Au: **(a)** with too few cracks, **(b)** with one crack from each geometrical feature, and **(c)** with too many cracks. The region of interest is that in the middle of the micrographs, between the geometrical features. This region is elevated to isolate it from the surrounding material. The cracks that can be seen in the exterior region were triggered from random flaws elsewhere in the system; they have no effect on the array of interest. The buckling patterns that can be seen are induced by Poisson's ratio effects and stress relaxation from the cracks. The dark shadows correspond to surface depressions in the strained film, and to the edges of the elevated region between the geometrical features.

Figure 11: A schematic of a structure showing cracks and geometrical features. Elliptical features with major and minor axes a and b are separated by a distance S_o. Flaws are introduced along the free edge of the

structure with a density ρ, with a statistical variation in crack length. The energy-release rate is based on the length of an individual crack and the distance to its nearest neighbor, as defined in this figure.

Figure 12: A plot showing cumulative distribution functions of the natural crack spacing in a structure with no geometrical features at different strains, for the limiting case of a very dense and long flaw population.

Figure 13: A plot showing the relationship between the mean crack spacing and the applied strain for a structure with no artificial features, as a function of the flaw population (described by different values of the density and characteristic flaw size).

Figure 14: Plots showing the three regimes corresponding to Fig. 4 for systems with a sufficient density of large intrinsic defects. These plots show the effect of changing the spacing, S_o/h, and aspect ratio, a/b, of the geometrical features. In **(a)**, $S_o/h = 10$ and $a/b = 2$; in **(b)**, $S_o/h = 10$ and $a/b = 5$; in **(c)**, $S_o/h = 50$ and $a/b = 2$. In **(a)** and **(b)**, the separation of the geometrical features is small, which allows a relatively wide strain range for the second regime. It will be noted that the aspect ratio of the features, is not particularly significant. In **(c)**, the onset of the second regime occurs just above the critical strain for a single crack to channel across the specimen, and a very narrow strain range is allowed for the second regime; again, consistent with Fig. 4.

Figure 15: Plots showing the effects of the aspect ratio, a/b, and spacing, S_o/h, of geometrical features on the cumulative distribution of the resultant crack arrays. In **(a)**, the crack spacing is $S_o/h = 10$, and in **(b)**, the crack spacing is $S_o/h = 50$. The short defects results in the require-

ment of a relatively high strain to get a uniform pattern. This strain is sensitive to the aspect ratio, and, at low aspect ratios, it can be much larger than that required to create uniform arrays when the flaws are very long. This results in unstable crack arrays, since any single relatively long flaws between the geometrical features can initiate a channel crack, and break the periodicity. Sharper aspect ratios for the geometrical features lower the strain required to generate uniform flaws. In the limiting case of very sharp features, the critical strains would be reduced to the level of those in Fig. 14.

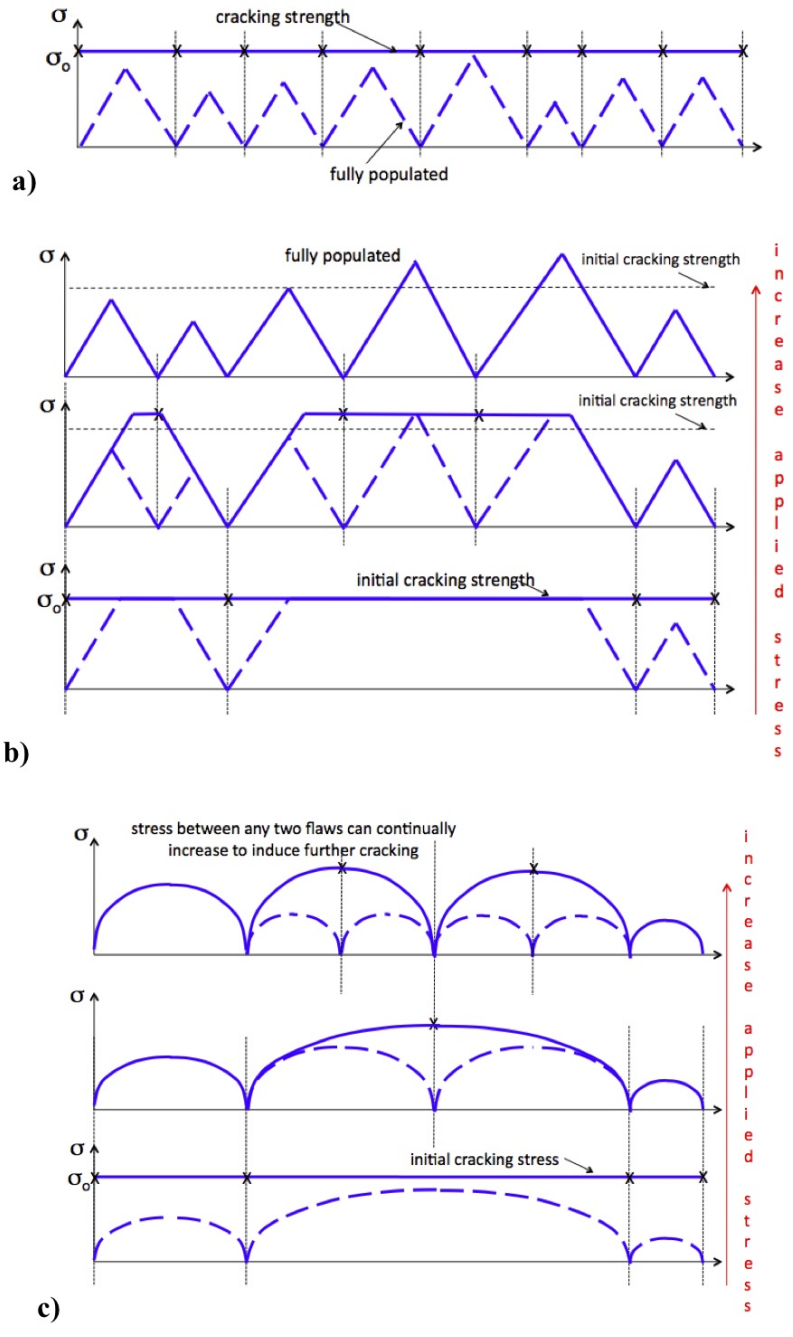
σ
cracking strength
σo
fully populated
a)
σ
fully populated
initial cracking strength
σ
initial cracking strength
σ
σo
initial cracking strength
increase applied stress
b)
σ
stress between any two flaws can continually increase to induce further cracking
σ
σ
σo
initial cracking stress
increase applied stress
c)

Figure 1:

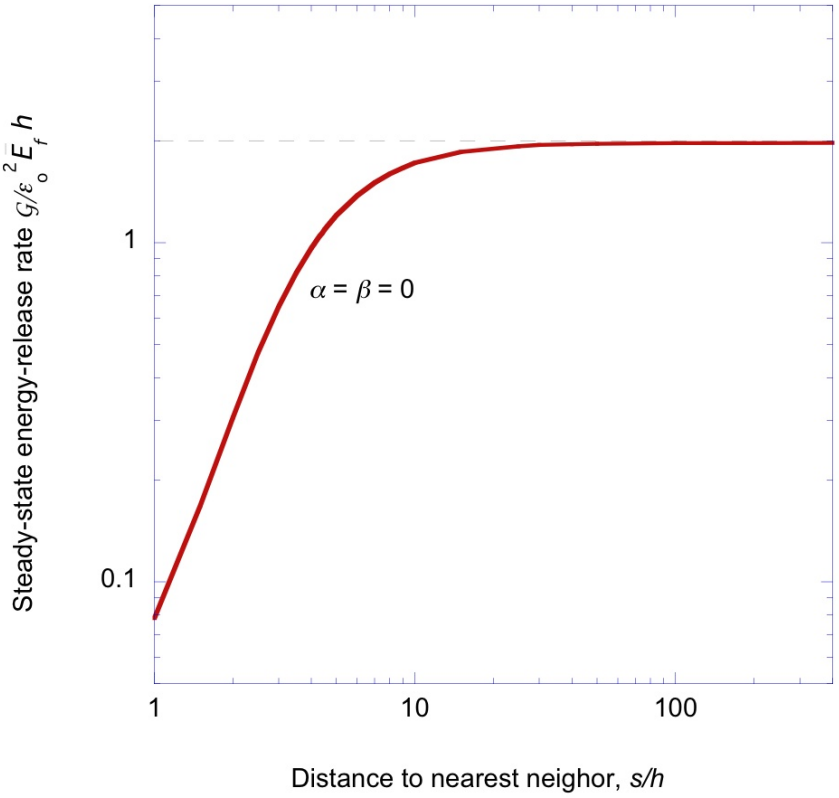
Steady-state energy-release rate $\mathcal{G}/\varepsilon_o^2 \bar{E}_f h$
1
0.1
$\alpha = \beta = 0$
1
10
100
Distance to nearest neighor, *s/h*

Figure 2:

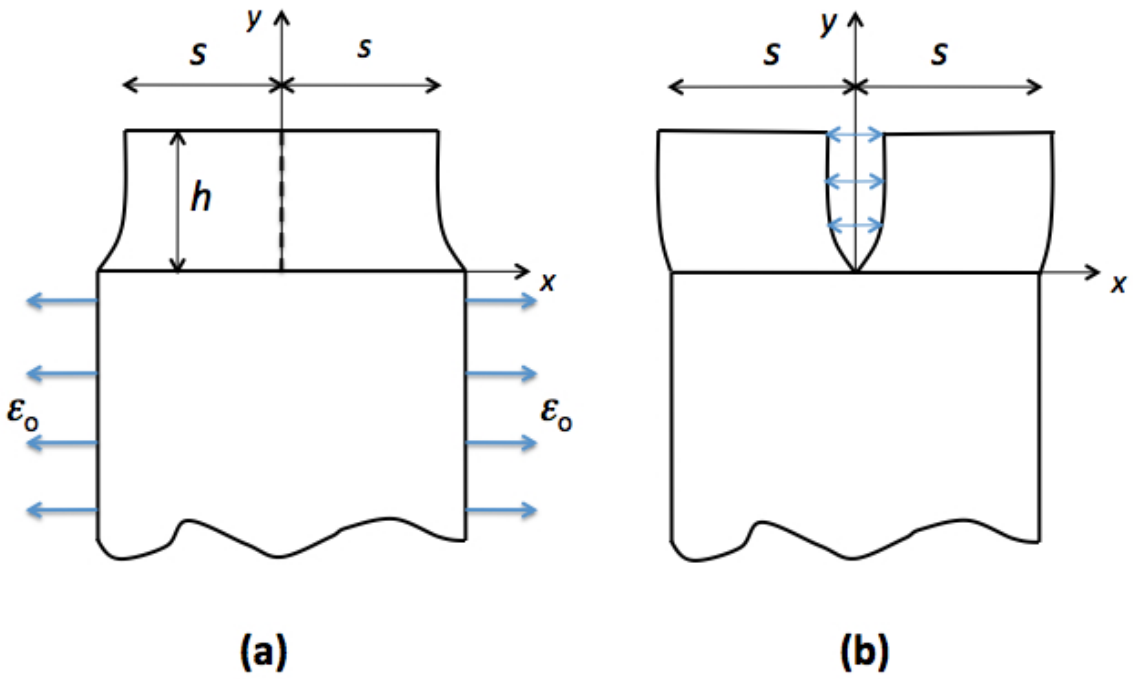

Figure 3:

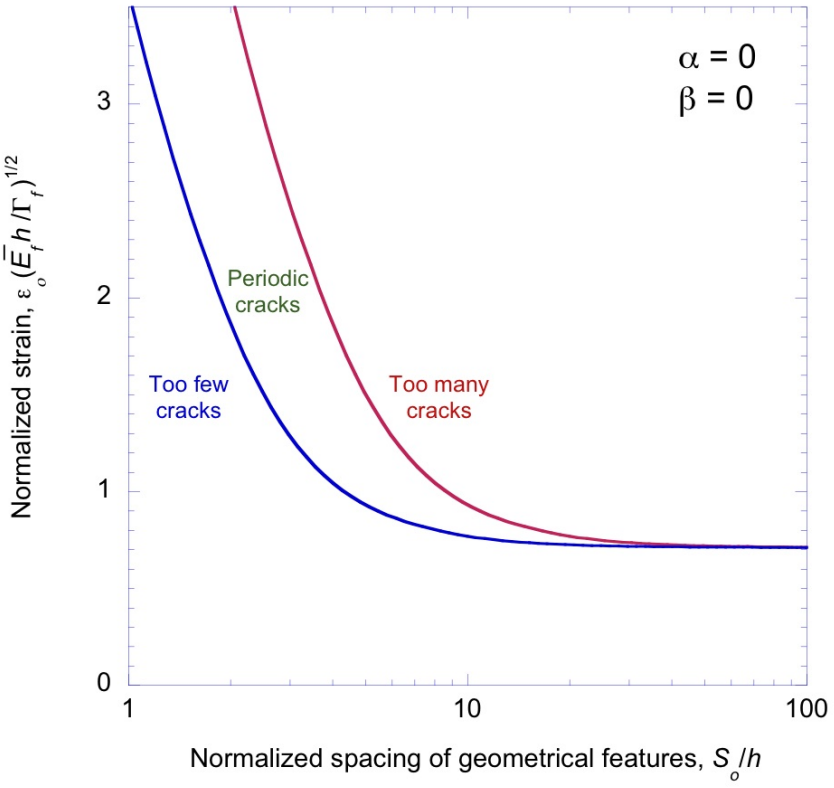
α = 0
β = 0
Periodic cracks
Too few cracks
Too many cracks
Normalized strain, $\varepsilon_o(\bar{E}_f h/\Gamma_f)^{1/2}$
Normalized spacing of geometrical features, S_o/h
0
1
2
3
1
10
100

Figure 4: (a)

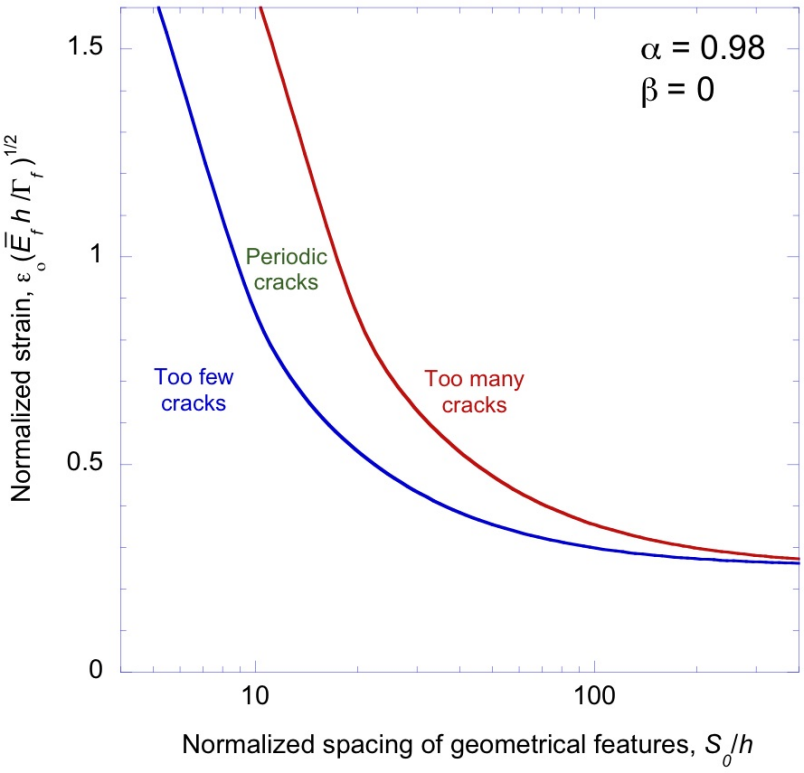
α = 0.98
β = 0
Periodic cracks
Too few cracks
Too many cracks
1.5
1
0.5
0
10
100
Normalized strain, $\varepsilon_o(\bar{E}_f h/\Gamma_f)^{1/2}$
Normalized spacing of geometrical features, S_0/h

Figure 4: (b)

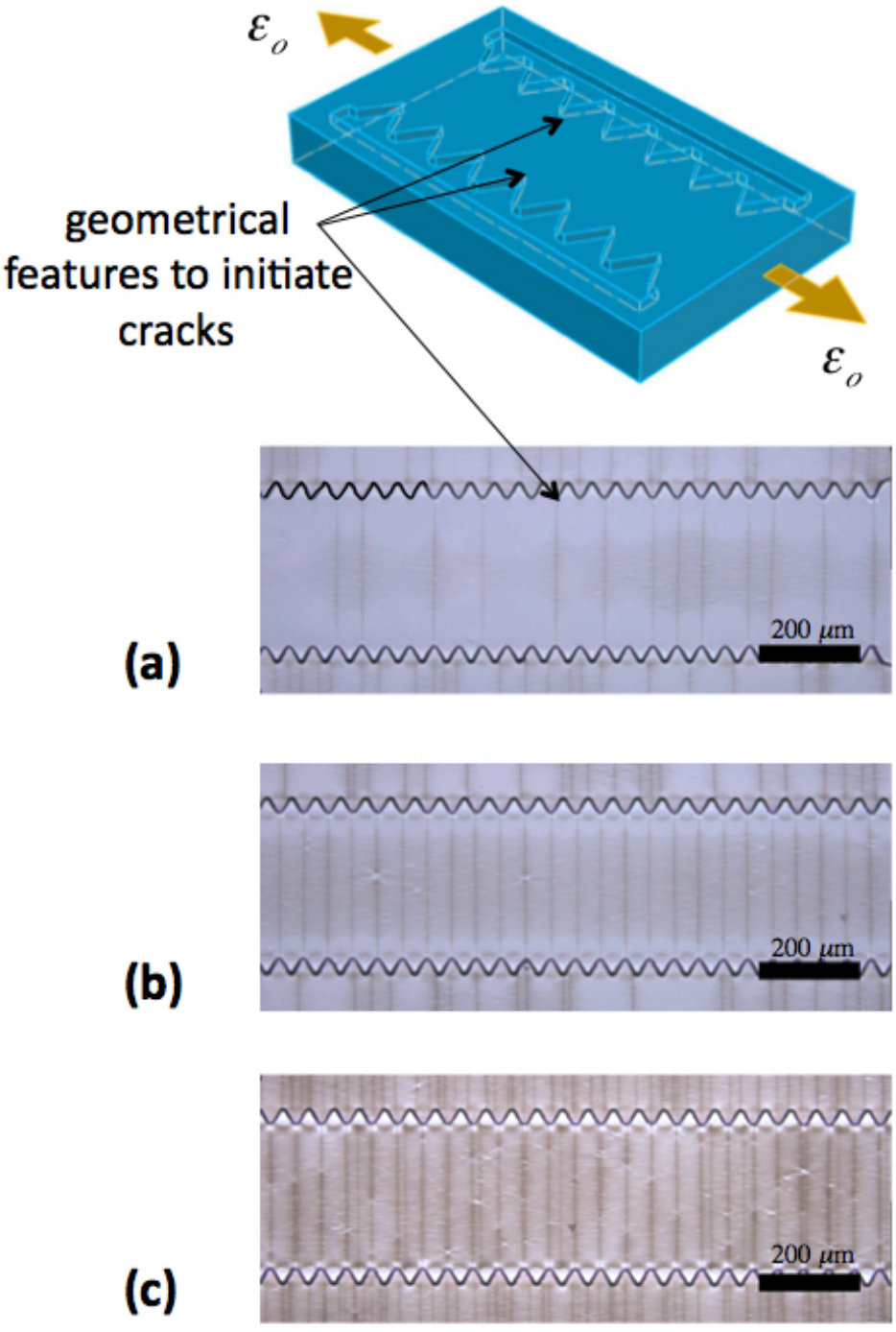
ε_o
geometrical features to initiate cracks
ε_o
200 μm
(a)
200 μm
(b)
200 μm
(c)

Figure 5:

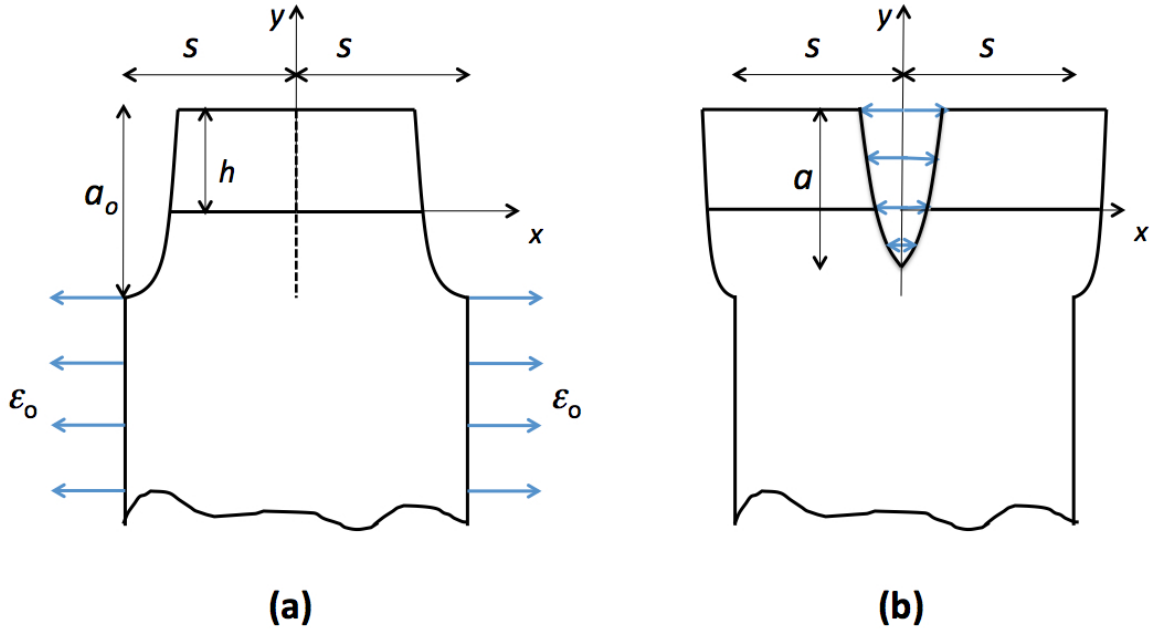

Figure 6:

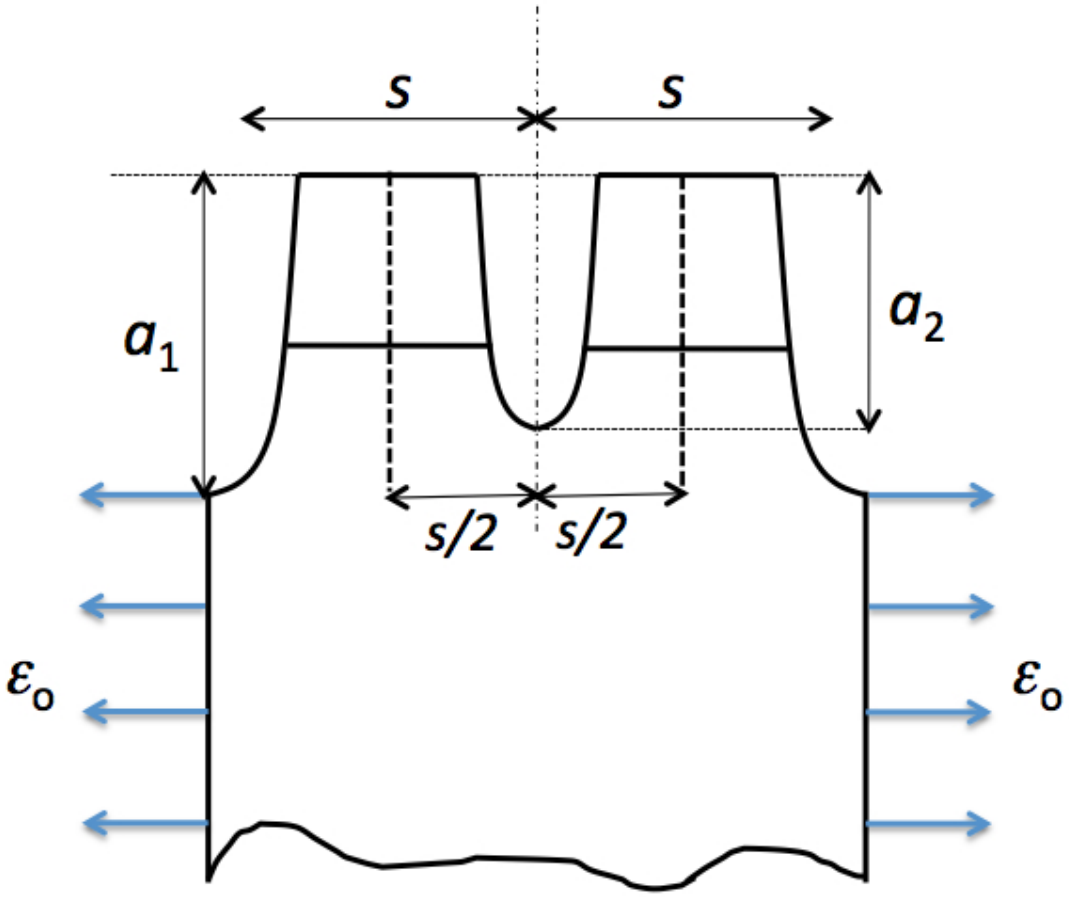

Figure 7:

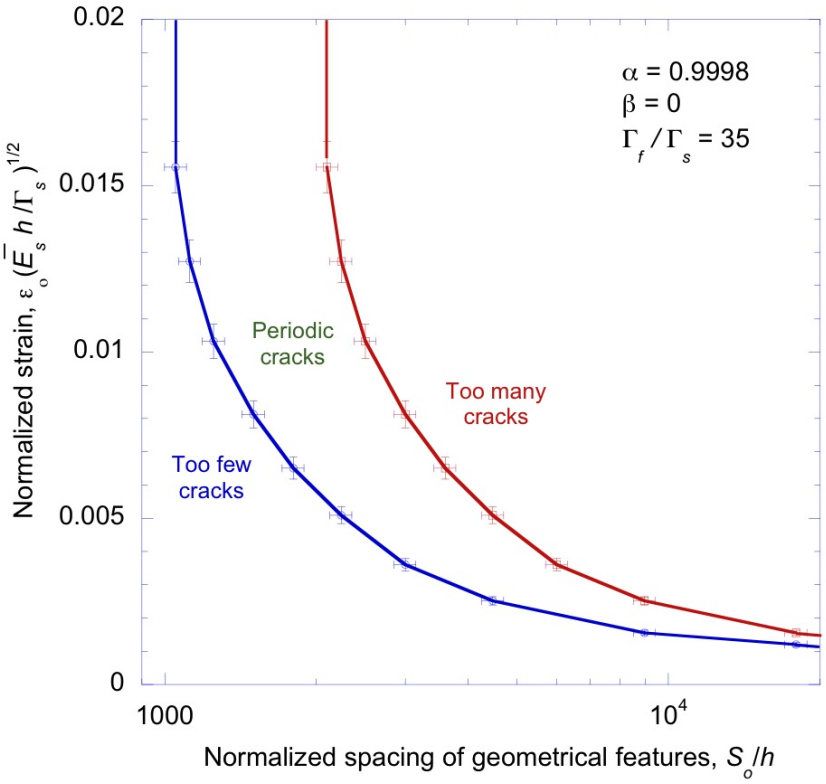
0.02
0.015
0.01
0.005
0
1000
10^4
Normalized strain, $\varepsilon_o (\bar{E}_s h/\Gamma_s)^{1/2}$
Normalized spacing of geometrical features, S_o/h
α = 0.9998
β = 0
Γ_f / Γ_s = 35
Periodic cracks
Too many cracks
Too few cracks

Figure 8:

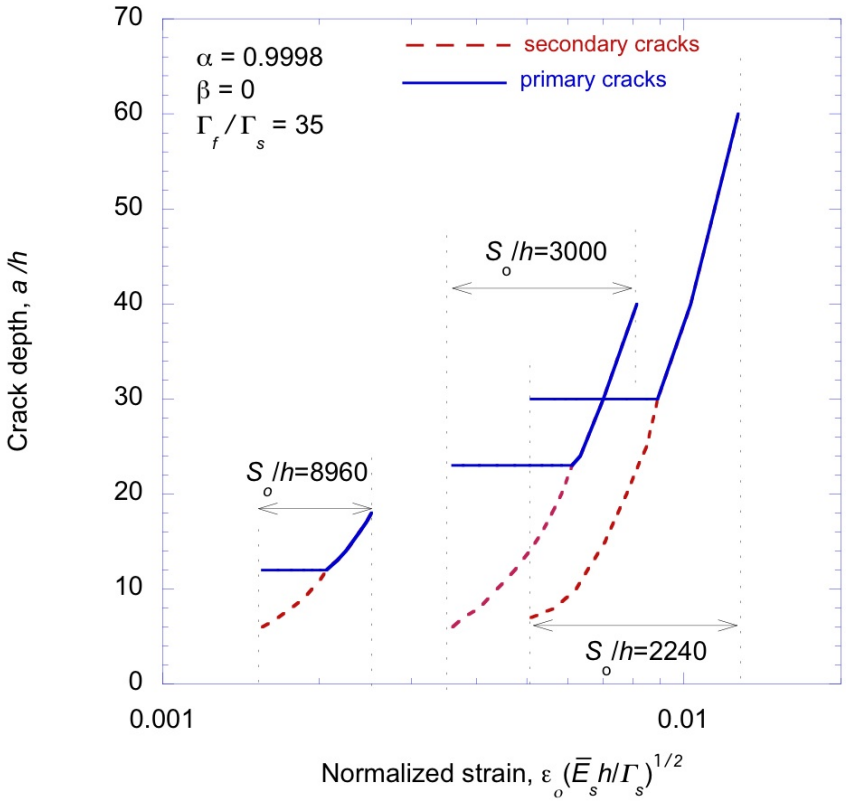
70
60
50
40
30
20
10
0
0.001
0.01
Crack depth, a /h
Normalized strain, ε o (Ē s h/Γ s)^1/2
α = 0.9998
β = 0
Γ f / Γ s = 35
secondary cracks
primary cracks
S o /h=3000
S o /h=8960
S o /h=2240

Figure 9:

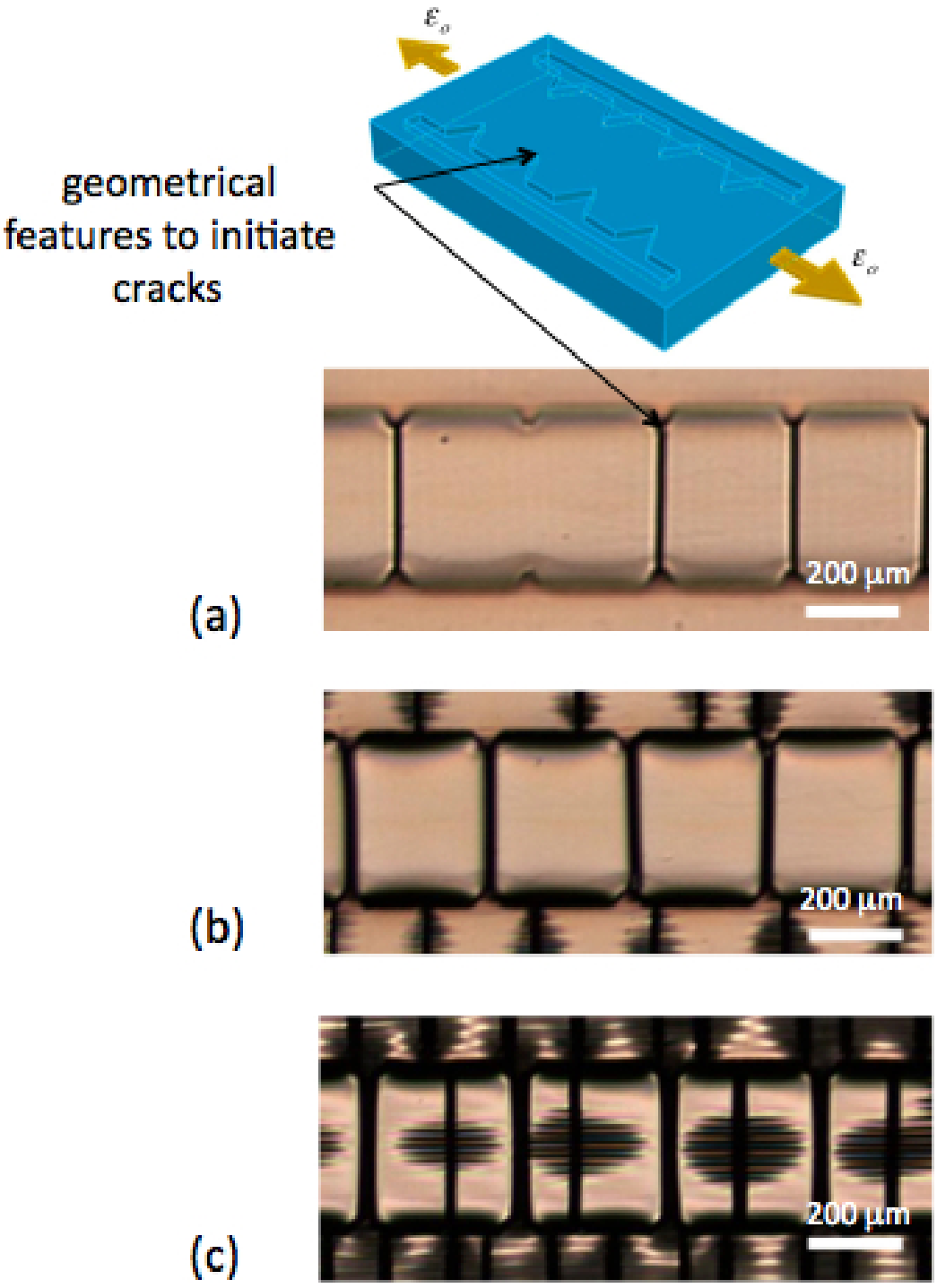
geometrical features to initiate cracks
ε_o
ε_o
200 µm
(a)
200 µm
(b)
200 µm
(c)

Figure 10:

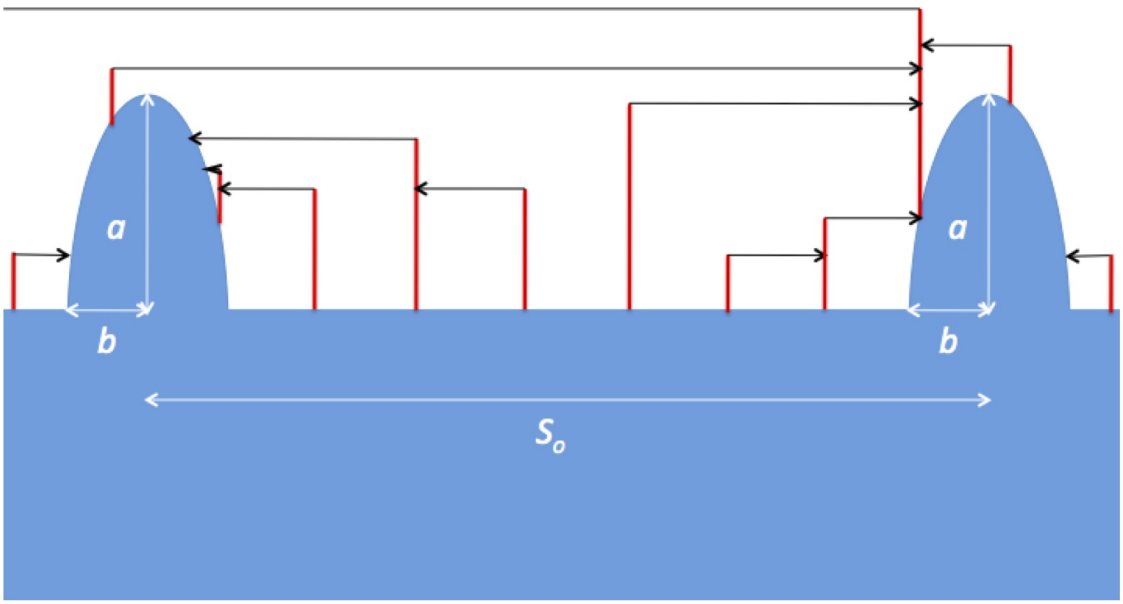

Figure 11:

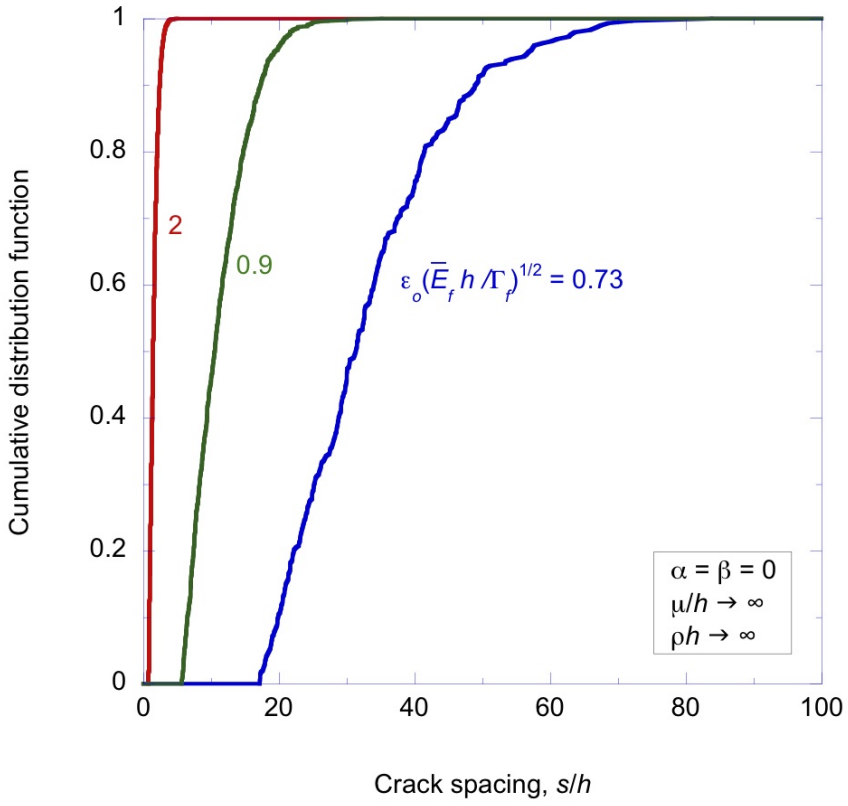
Cumulative distribution function
Crack spacing, s/h
1
0.8
0.6
0.4
0.2
0
0
20
40
60
80
100
2
0.9
$\varepsilon_o(\bar{E}_f h/\Gamma_f)^{1/2} = 0.73$
$\alpha = \beta = 0$
$\mu/h \to \infty$
$\rho h \to \infty$

Figure 12:

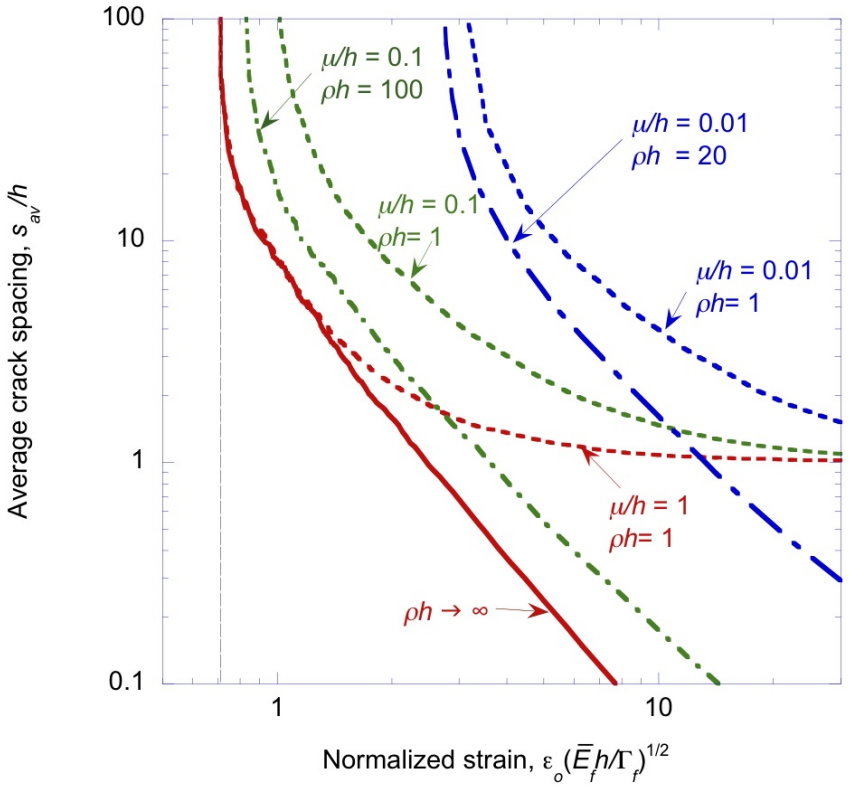
100
10
1
0.1
1
10
Average crack spacing, s_{av}/h
Normalized strain, $\varepsilon_o(\bar{E}_f h/\Gamma_f)^{1/2}$
μ/h = 0.1
ρh = 100
μ/h = 0.01
ρh = 20
μ/h = 0.1
ρh= 1
μ/h = 0.01
ρh= 1
μ/h = 1
ρh= 1
$\rho h \to \infty$

Figure 13:

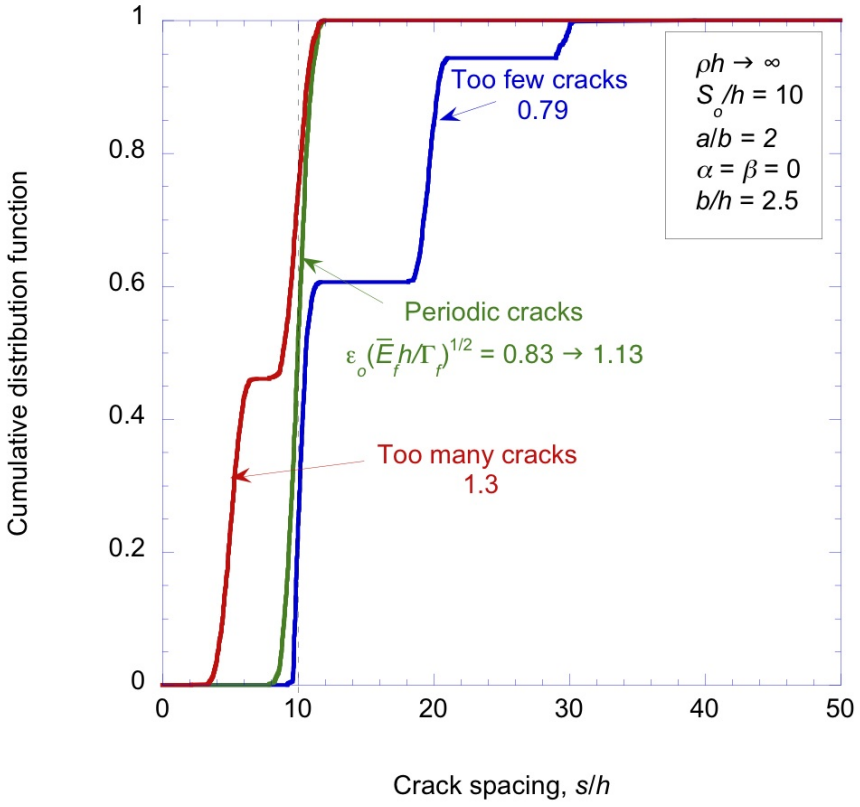
Cumulative distribution function
Crack spacing, s/h
Too few cracks
0.79
Periodic cracks
$\varepsilon_o(\bar{E}_f h/\Gamma_f)^{1/2} = 0.83 \rightarrow 1.13$
Too many cracks
1.3
$\rho h \rightarrow \infty$
$S_o/h = 10$
$a/b = 2$
$\alpha = \beta = 0$
$b/h = 2.5$
0
0.2
0.4
0.6
0.8
1
0
10
20
30
40
50

Figure 14: (a)

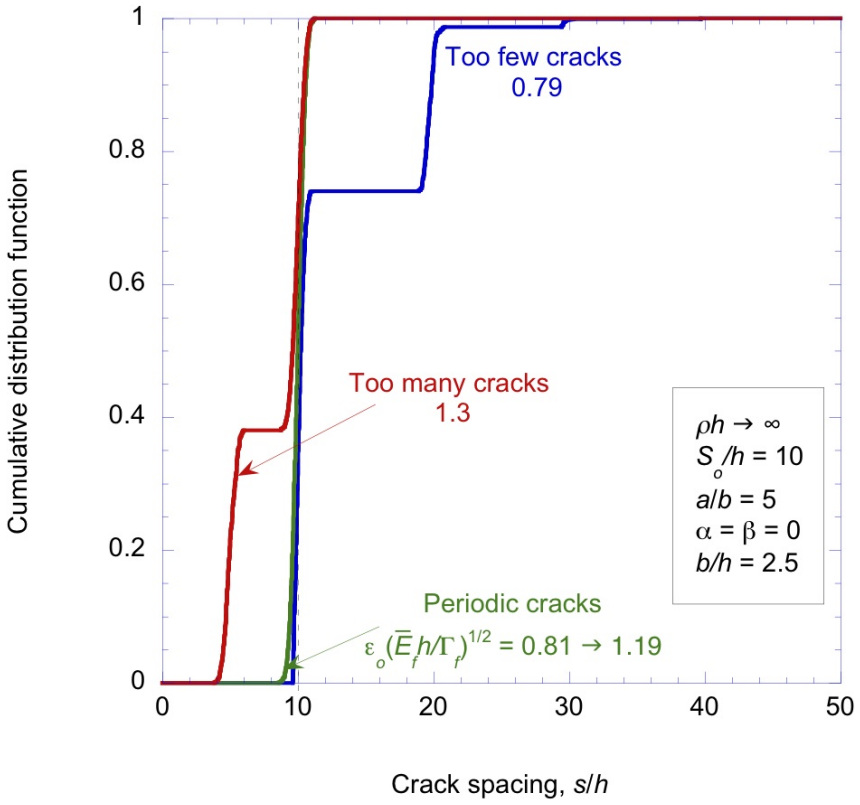
Too few cracks
0.79
Too many cracks
1.3
Periodic cracks
$\varepsilon_o(\bar{E}_f h/\Gamma_f)^{1/2} = 0.81 \rightarrow 1.19$
$\rho h \rightarrow \infty$
$S_o/h = 10$
$a/b = 5$
$\alpha = \beta = 0$
$b/h = 2.5$
Cumulative distribution function
Crack spacing, s/h
0
0.2
0.4
0.6
0.8
1
0
10
20
30
40
50

Figure 14: (b)

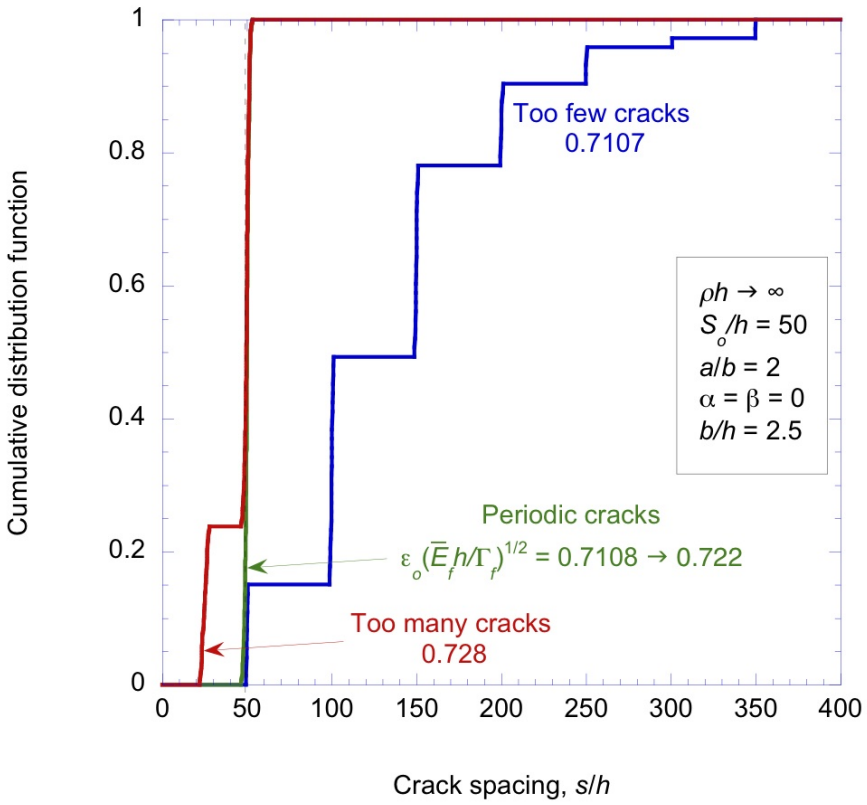
Cumulative distribution function
Crack spacing, s/h
Too few cracks
0.7107
ρh → ∞
S_o/h = 50
a/b = 2
α = β = 0
b/h = 2.5
Periodic cracks
ε_o(Ē_f h/Γ_f)^1/2 = 0.7108 → 0.722
Too many cracks
0.728
0
0.2
0.4
0.6
0.8
1
0
50
100
150
200
250
300
350
400

Figure 14: (c)

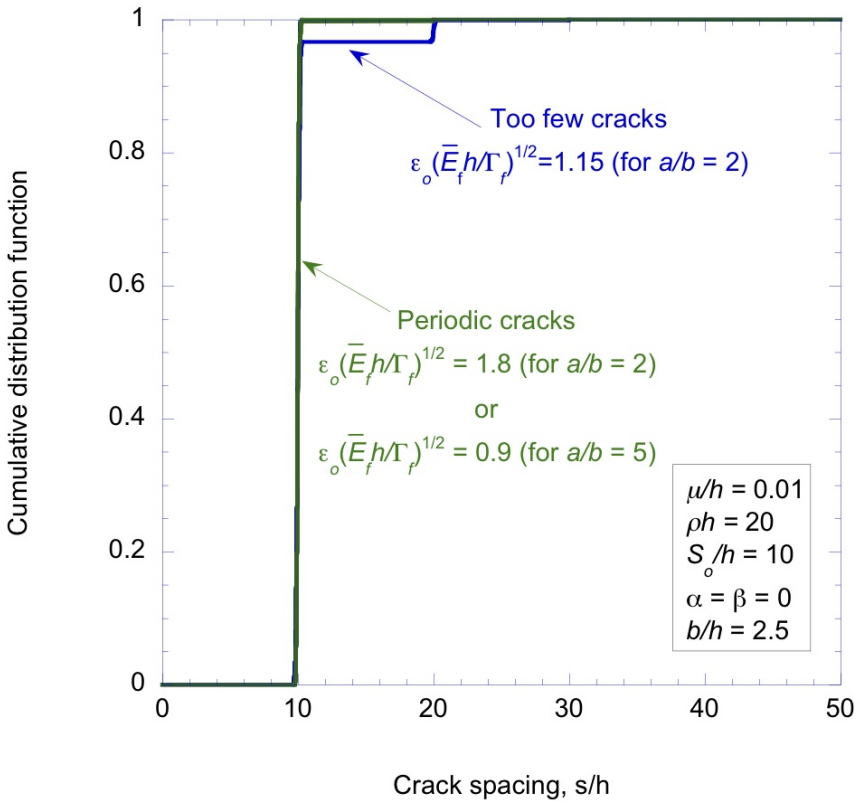
Cumulative distribution function
Crack spacing, s/h
Too few cracks
$\varepsilon_o(\bar{E}_f h/\Gamma_f)^{1/2}$=1.15 (for a/b = 2)
Periodic cracks
$\varepsilon_o(\bar{E}_f h/\Gamma_f)^{1/2}$ = 1.8 (for a/b = 2)
or
$\varepsilon_o(\bar{E}_f h/\Gamma_f)^{1/2}$ = 0.9 (for a/b = 5)
μ/h = 0.01
ρh = 20
S_o/h = 10
$\alpha = \beta$ = 0
b/h = 2.5
0
0.2
0.4
0.6
0.8
1
0
10
20
30
40
50

Figure 15: (a)

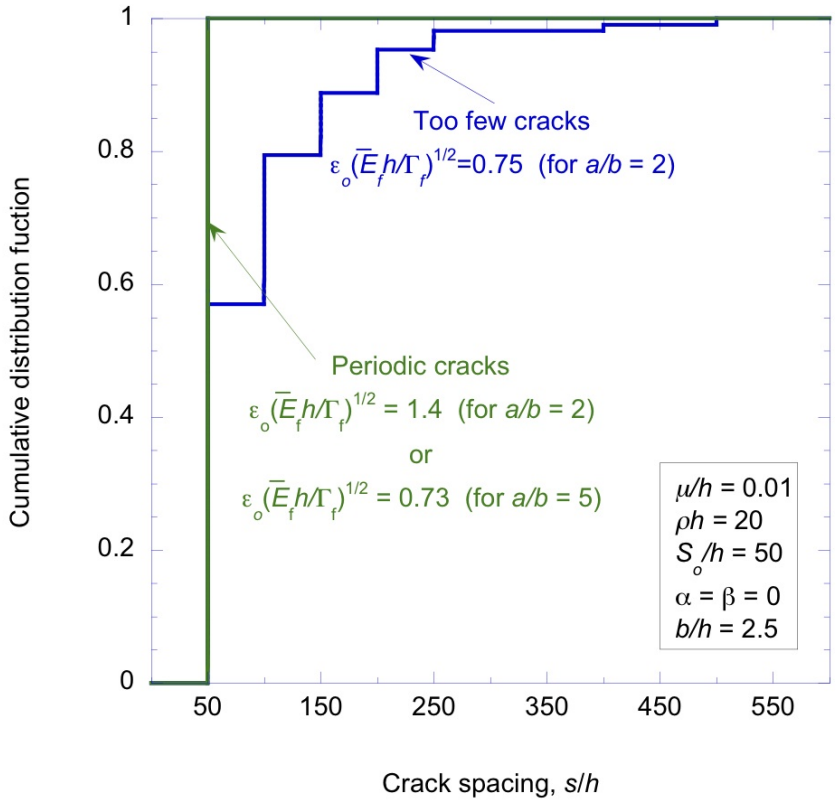
Cumulative distribution fuction
1
0.8
0.6
0.4
0.2
0
50
150
250
350
450
550
Crack spacing, s/h
Too few cracks
ε_o(Ē_f h/Γ_f)^1/2=0.75 (for a/b = 2)
Periodic cracks
ε_o(Ē_f h/Γ_f)^1/2 = 1.4 (for a/b = 2)
or
ε_o(Ē_f h/Γ_f)^1/2 = 0.73 (for a/b = 5)
μ/h = 0.01
ρh = 20
S_o/h = 50
α = β = 0
b/h = 2.5

Figure 15: (b)